Journal of Sound and Vibration (2002) **251**(4), 697–716
doi:10.1006/jsvi.2001.3996, available online at http://www.idealibrary.com on IDEAL®

DYNAMIC LOAD ON CONTINUOUS MULTI-LANE BRIDGE DECK FROM MOVING VEHICLES

X. Q. Zhu and S. S. Law

Civil and Structural Engineering Department, Hong Kong Polytechnic University, Hung Hom, Hong Kong, People's Republic of China. E-mail:cesslaw@polyu.edu.hk

(*Received* 16 *January* 2001, *and in final form* 25 *July* 2001)

The dynamic loading on a multi-lane continuous bridge deck due to vehicles moving on top at a constant velocity is investigated. The bridge is modelled as a multi-span continuous orthotropic rectangular plate with line rigid intermediate supports. The vehicle is simulated as a two-axle three-dimensional vehicle model with seven degrees of freedom according to the H20-44 vehicle design loading (*AASHTO LRFD Bridge Design Specifications* 1998 American Association of State Highway and Transportation Officials [1]). The dynamic behavior of the bridge deck under single and several vehicles moving in different lanes is analyzed using the orthotropic plate theory and modal superposition technique. The dynamic loading is studied in terms of the dynamic impact factor of the bridge deck. The impact factor is found varying in an opposite trend as the dynamic responses for the different loading cases under study.

1. INTRODUCTION

Dynamic loading on bridges caused by moving vehicles on top is an important factor in the design and structural evaluation of the bridges, and many research results have been published in the last few decades. There are three methods to simulate the dynamic interaction between the bridge and vehicles. The iterative method [2–9] solved the two uncoupled sets of equation for the bridge and vehicles separately by an iterative procedure to satisfy the geometrical compatibility conditions and equilibrium conditions of the interaction forces between the bridge and vehicle. The second method constructs the coupled equations of equilibrium using a modal superposition method in a Lagrangian formulation, and direct time integration is used to solve the coupled equations [10]. Yang *et al.* [11] developed a vehicle–bridge interaction element for the dynamic analysis of the bridge under moving vehicles. The interaction element consists of a bridge element and the suspension units of the vehicle resting on top of the element.

Generally, the dynamic loading obtained above is incorporated into the structural design in the form of a dynamic amplification factor, defined as the ratio of the maximum dynamic response to the maximum static response. The impact factor is influenced by many variables, such as the dynamic properties of the bridge and the vehicle, the road surface roughness and the surface condition of the approach, the number of travelling vehicles and their transverse positions, and vehicle braking or acceleration on top of the bridge. Cantieni [12] studied the vehicle–bridge interaction in his field tests. Hwang and Nowak [13] developed a procedure for calculation of the dynamic load and it is subsequently used in the development of a reliability based design code. The dynamic response of a single span

0022-460X/02/140697 + 20 $35.00/0

multi-girder bridge deck under a single vehicle and two vehicles moving with different speeds is studied by Wang *et al.* [3] using grillage beam theory. Huang *et al.* [2] extended this method to analyze the impact factor of continuous multigirder bridges due to moving vehicles. Chatterjee *et al.* [5] simplified the continuous bridge deck as a continuous Euler–Bernoulli beam with torsional vibration, and a quarter truck model is used in the simulations. Yang *et al.* [14] discussed the effects of the speed parameter, the vehicle/bridge frequency ratio, and damping of the bridge and road roughness on the impact factors. The influencing parameters on the dynamic behavior of a three-dimensional bridge are studied by Kou and Dewolf [15] using the finite-element method.

This paper investigates the dynamic loading on a multi-lane continuous bridge due to vehicles moving on top of the bridge deck. The bridge is modelled as a multi-span continuous orthotropic rectangular plate with intermediate line rigid supports. The analytical vehicle is simulated as a two-axle three-dimensional vehicle model with seven degrees of freedom according to the H20-44 vehicle design loading in AASHTO [1]. The dynamic behavior of the bridge under several moving vehicles is analyzed using orthotropic plate theory and modal superposition technique. The effects of multi-lane loading from multiple vehicles on the dynamic impact factor of the bridge are discussed. The impact factor is found varying in an opposite trend as the dynamic responses for the different loading cases under study.

2. DYNAMIC BEHAVIOR OF BRIDGE DECK UNDER MOVING VEHICLES

2.1. ASSUMPTIONS

The following assumptions are made for the formulation of the problem.

(1) The bridge is treated as a continuous rectangular orthotropic plate with simple supports at its two ends ($x = 0, a$), and the other two opposite edges are free ($y = 0, b$) as shown in Figure 1. A linear elastic behavior is assumed, and the effects of shear deformation and rotary inertia are neglected.
(2) The intermediate line supports of the bridge are assumed as linear rigid and they are orthogonal to the free edges of the plate.
(3) The model for the H20-44 truck loading comprises three rigid masses which represent the truck body, front and rear wheel/axle set, respectively, as shown in Figure 2.
(4) Since the horizontal dimension of the bridge deck is much larger than its thickness, the thin plate assumption is made.

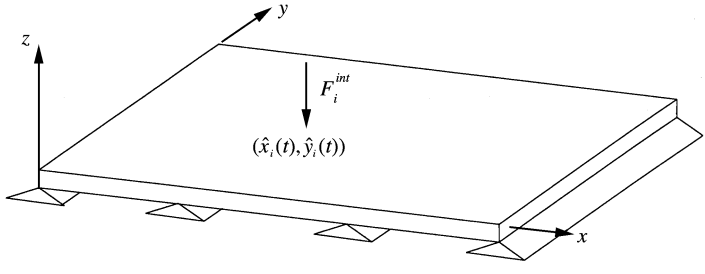

Figure 1. Model of the continuous bridge deck.

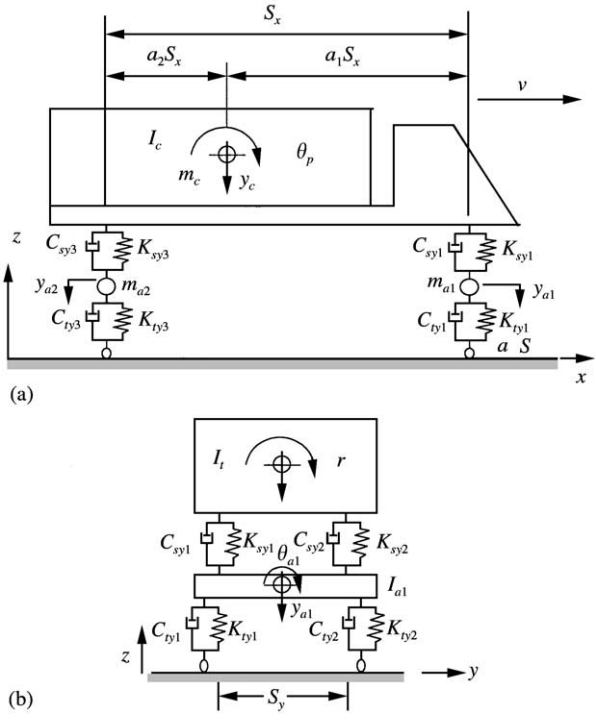

Figure 2. Idealization of two-axle vehicle. (a) Elevation; (b) cross-sectional view at front axle.

2.2. VIBRATION OF THE BRIDGE DECK

From the vibrational theory of thin plate, the strain energy of the continuous orthotropic plate in Cartesian co-ordinates is

$$U_e = \iiint_V \frac{1}{2}\sigma_i \varepsilon_i \, \mathrm{d}V$$

$$= \frac{1}{2}\iint_S \left[D_x \left(\frac{\partial^2 w}{\partial x^2}\right)^2 + (D_x v_{yx} + D_y v_{xy}) \frac{\partial^2 w}{\partial x^2}\frac{\partial^2 w}{\partial y^2} + D_y \left(\frac{\partial^2 w}{\partial y^2}\right)^2 + 4D_k \left(\frac{\partial^2 w}{\partial x \partial y}\right)^2 \right] \mathrm{d}S, \quad (1)$$

where D_x, D_y, D_k are the rigidity constants of the orthotropic plate; v_{yx}, v_{xy} are the Poisson ratio of the orthotropic material. For the bridge deck with material orthotropy and an equivalent uniform plate thickness h, $D_x = E_x h^3/12(1 - v_{xy}v_{yx})$, $D_y = E_y h^3/12(1 - v_{xy}v_{yx})$, $D_k = G_{xy}h^3/12$, in which E_x, E_y are Young's moduli in the x and y directions, respectively, G_{xy} is the shear modulus. These rigidities can be determined by the method of Bakht and Jaeger [16].

The kinetic energy of the system is expressed as

$$T = \frac{1}{2}\iint_S \rho h \left(\frac{\partial w}{\partial t}\right)^2 \mathrm{d}S, \quad (2)$$

where ρ is the mass density of plate material, and w is the vertical deflection.

The work done by the damping of the plate and moving loads are as follows:

$$W_c = -\iint_S c_b w \frac{\partial w}{\partial t} \mathrm{d}S,$$

$$W_e = \iint_S \sum_{N_f} F_i^{int} \delta(x - \hat{x}_i(t)) \delta(y - \hat{y}_i(t)) w \, \mathrm{d}S, \tag{3}$$

where c_b is the damping coefficient of the plate; F_i^{int} is the ith interaction force between the vehicular wheel and the bridge. $(\hat{x}_i(t), \hat{y}_i(t))$ is the location of the interaction force F_i^{int}. When the vehicle is moving along one lane, $\hat{y}_i$(t) is a constant. $\delta(x), \delta(y)$ are the Dirac functions.

Based on modal superposition, the dynamic deflection $w(x, y, t)$ can be described as

$$w(x, y, t) = \sum_{i=0}^{\infty} W_i(x, y) q_i(t), \tag{4}$$

where $W_i(x, y)$ is the vibration mode shape of the plate and $q_i(t)$ is the corresponding modal amplitude. When equation (4) is substituted into equations (1)–(3), the equations of motion for the bridge are

$$\mathbf{M}_b \ddot{\mathbf{Q}} + \mathbf{C}_b \dot{\mathbf{Q}} + \mathbf{K}_b \mathbf{Q} = \mathbf{W}_b \mathbf{F}_b^{int}, \tag{5}$$

where $\mathbf{M}_b$, $\mathbf{C}_b$, $\mathbf{K}_b$ are the mass, damping and stiffness matrices of the bridge, respectively (Appendix A); $\mathbf{F}_b^{int}$ is the vector of interaction force under the wheels of the moving vehicles. $\dot{\mathbf{Q}}$, $\ddot{\mathbf{Q}}$ are the first and second derivatives of $\mathbf{Q}$ and $\mathbf{Q}$ is the vector of modal amplitudes.

2.3. MODAL ANALYSIS OF THE BRIDGE DECK

For free vibration of the plate, the vertical displacement may be expressed as

$$w(x, y, t) = W(x, y) \mathrm{e}^{\mathrm{j}\omega t}, \tag{6}$$

where ω is the natural frequency of vibration and $\mathrm{j} = \sqrt{-1}$. Assuming the variables in $W(x, y)$ are separable, the mode shape function $W(x, y)$ can be expressed in terms of a series as

$$W(x, y) = \sum_m \sum_n A_{mn} \varphi_m(x) \psi_n(y), \tag{7}$$

where $\varphi_m(x)$ and $\psi_n(y)$ are the assumed admissible functions along the x and y directions respectively, while A_{mn} are the unknown coefficients. A set of series consisting of a combination of beam eigenfunctions and polynomials has been selected as the admissible functions of the line-supported plates by Zhou [17]. Here we take $\varphi_m(x)$ to be the eigenfunctions of the continuous multi-span Euler–Bernoulli beam, and $\psi_n(y)$ are the eigenfunctions of the single-span Euler–Bernoulli beam satisfying the free boundary conditions. Substituting equation (7) into equations (6), (1)–(3), and taking the first

derivative of the Rayleigh's quotient with respect to each coefficient A_{mn} would lead to the eigenvalue equations in matrix form as follows:

$$(\mathbf{K}_b - \omega^2 \mathbf{M}_b)\mathbf{A} = 0, \tag{8}$$

where

$$\begin{aligned}
A &= \{A_{11}, A_{12}, \ldots, A_{1N}, A_{21}, \ldots, A_{MN}\}^{\mathrm{T}};\\
m_{bij} &= \rho h \int_0^a \varphi_{m1}(x)\varphi_{m2}(x)\,\mathrm{d}x \int_0^b \psi_{n1}(y)\psi_{n2}(y)\,\mathrm{d}y,\\
k_{bij} &= D_x \int_0^a \varphi''_{m1}(x)\varphi''_{m2}(x)\,\mathrm{d}x \int_0^b \psi_{n1}(y)\psi_{n2}(y)\,\mathrm{d}y\\
&\quad + D_y \int_0^a \varphi_{m1}(x)\varphi_{m2}(x)\,\mathrm{d}x \int_0^b \psi''_{n1}(y)\psi''_{n2}(y)\,\mathrm{d}y\\
&\quad + v_{xy} D_y \left(\int_0^a \varphi''_{m1}(x)\varphi_{m2}(x)\,\mathrm{d}x \int_0^b \psi_{n1}(y)\psi''_{n2}(y)\,\mathrm{d}y \right.\\
&\quad \left. + \int_0^a \varphi_{m1}(x)\varphi''_{m2}(x)\,\mathrm{d}x \int_0^b \psi''_{n1}(y)\psi_{n2}(y)\,\mathrm{d}y \right)\\
&\quad + 2(1 - v_{xy}) D_{xy} \int_0^a \varphi'_{m1}(x)\varphi'_{m2}(x)\,\mathrm{d}x \int_0^b \psi'_{n1}(y)\psi'_{n2}(y)\,\mathrm{d}y\\
&\quad (m1 = 1, 2, \ldots, M;\ m2 = 1, 2, \ldots, M; \quad n1 = 1, 2, \ldots, N; \quad n2 = 1, 2, \ldots, N)\\
&\quad i = (m1 - 1)N + n1; \quad j = (m2 - 1)N + n2
\end{aligned} \tag{9}$$

and M, N are the number of admissible functions in x and y directions respectively. $\varphi''_m(x)$, $\varphi'_m(x)$ are the second and first derivatives of $\varphi_m(x)$; $\psi''_n(y)$, $\psi'_n(y)$ are the second and first derivatives of $\psi_n(y)$.

The natural frequencies ω and coefficients A_{mn} can be determined from equation (8). Then the mode shape functions of the continuous orthotropic plate are also determined from equation (7). Since the admissible functions are eigenfunctions of the Euler–Bernolli beam, the mode shape functions of the continuous orthotropic plate satisfy the orthogonality relationships. It should be noted that this approach is much more simple and direct than the existing methods by Zhou [17] and Marchesiello *et al.* [8].

2.4. VEHICLE MODEL

The mathematical model for the H20-44 truck is shown in Figure 2. The model is similar to that employed by Marchesiello *et al.* [8]. The vehicular body is assigned three degrees of freedom, corresponding to the vertical displacement (y), rotation about the transverse axis (pitch or θ_p), and rotation about the longitudinal axis (roll or θ_r). Each wheel/axle set is provided with two degrees of freedom in the vertical and roll directions (y_{a1}, y_{a2}, θ_{a1}, θ_{a2}).

Therefore, the total number of independent degrees of freedom is seven. The equations of motion of the vehicle are derived using Lagrange's formulation as follows:

$$\mathbf{M}_v\ddot{\mathbf{Z}} + \mathbf{C}_v\dot{\mathbf{Z}} + \mathbf{K}_v\mathbf{Z} = \mathbf{F}_v^{int}, \tag{10}$$

where $\mathbf{F}_v^{int}$ is the interaction force vector applied on the vehicle; $\mathbf{M}_v$, $\mathbf{C}_v$, $\mathbf{K}_v$ are, respectively, the mass, damping and stiffness matrices of the vehicle system and $\mathbf{Z}$ is the vector of the vehicle degrees of freedom (Appendix A).

2.5. VEHICLE–BRIDGE INTERACTION

The vehicle-bridge interaction forces for a single vehicle can be written as follows:

$$\begin{aligned}
F_{t1} &= K_{ty1}(y_{a1} - \tfrac{1}{2}S_{d1}\theta_{a1} - w_1 - d_1) + C_{ty1}(\dot{y}_{a1} - \tfrac{1}{2}S_{d1}\dot{\theta}_{a1} - \dot{w}_1 - \dot{d}_1),\\
F_{t2} &= K_{ty2}(y_{a1} + \tfrac{1}{2}S_{d1}\theta_{a1} - w_2 - d_2) + C_{ty2}(\dot{y}_{a1} + \tfrac{1}{2}S_{d1}\dot{\theta}_{a1} - \dot{w}_2 - \dot{d}_2),\\
F_{t3} &= K_{ty3}(y_{a2} - \tfrac{1}{2}S_{d2}\theta_{a2} - w_3 - d_3) + C_{ty3}(\dot{y}_{a2} - \tfrac{1}{2}S_{d2}\dot{\theta}_{a2} - \dot{w}_3 - \dot{d}_3),\\
F_{t4} &= K_{ty4}(y_{a2} + \tfrac{1}{2}S_{d2}\theta_{a2} - w_4 - d_4) + C_{ty4}(\dot{y}_{a2} + \tfrac{1}{2}S_{d2}\dot{\theta}_{a2} - \dot{w}_4 - \dot{d}_4),
\end{aligned} \tag{11}$$

where $\{K_{tyi}, i = 1, 2, 3, 4\}$ are the stiffness of the tyres; $\{C_{tyi}, i = 1, 2, 3, 4\}$ are the damping coefficients of the tyres. S_{d1}, S_{d2} are the wheel spacing of the front and rear axles respectively.

$$w_i = w(\hat{x}_i(t), \hat{y}_i(t), t), \qquad d_i = d(\hat{x}_i(t), \hat{y}_i(t)); \quad i = 1, 2, 3, 4, \tag{12}$$

where $d(x, y)$ is the surface roughness of the bridge deck; $(\hat{x}_i(t), \hat{y}_i(t))$ is the location of the ith tyre at time t. As the vehicle moves along one lane, $\hat{y}_1(t) = y_0 + S_{d1}/2$, $\hat{y}_2(t) = y_0 - S_{d1}/2$, $\hat{y}_3(t) = y_0 + S_{d2}/2$, $\hat{y}_4(t) = y_0 - S_{d2}/2$, and y_0 is the transverse co-ordinate of the centerline of the lane.

The dynamic responses of the bridge deck under moving vehicles can be calculated from equations (5), (10) and (11) using an iterative method (such as the Newmark method) or the algorithm by Henchi *et al.* [10].

2.6. ROAD ROUGHNESS OF THE BRIDGE PAVEMENT

The randomness of the road surface roughness can be represented with a periodic modulated random process. In ISO-8608 [18] specifications, the road surface roughness is related to the vehicle speed by a formula between the velocity power spectral density (PSD) and the displacement PSD. The general form of the displacement PSD of the road surface roughness is given as

$$S_d(f) = S_d(f_0)(f/f_0)^{-\alpha} \tag{13}$$

where $f_0 (= 0{\cdot}1$ cycles/m) is the reference spatial frequency; α is an exponent of the PSD, and f is the spatial frequency (cycles/m). Equation (13) gives an estimate on the degree of

roughness of the road from the $S_d(f_0)$ value. This classification is made by assuming a constant vehicle velocity PSD, taking α equals to 2. The ISO specification also gives the power spectral densities for different classes of roads.

Based on this ISO specification, the road surface roughness in the time domain can be simulated by applying the inverse fast Fourier transformation on $S_d(f)$ as follows [10]:

$$r(x) = \sum_{i=1}^{N} \sqrt{4S(f_i)\Delta f}\cos(2\pi f_i x + \theta_i), \tag{14}$$

where $f_i = i\Delta f$ is the spatial frequency; $\Delta f = 1/N\Delta$; Δ is the distance interval between successive ordinates of the surface profile; N is the number of data points, and θ_i is a set of independent random phase angle uniformly distributed between 0 and 2π.

2.7. PROCEDURE OF IMPLEMENTATION

The coupled equations of motion of the bridge–vehicle system presented in equations (5) and (10) are subjected to the compatibility constraints on the interaction forces and the displacements of the two subsystems. The procedure to solve the problem is implemented as follows:

Step 1: Calculate the mode shapes and natural frequencies of the multi-span bridge deck
(1) Determine the assumed admissible functions $\varphi_m(x)$ and $\psi_n(y)$ in equation (7).
(2) Calculate the natural frequencies ω and the coefficients A_{mn} from equation (8). The mode shapes are determined by equation (7).

Step 2: Determine the mass, stiffness and damping matrices of both the vehicle and the bridge deck.

Step 3: Calculate the road surface roughness function $d(x)$ from equation (14) according to the selected road class in ISO-8608 [18].

Step 4: The responses of the bridge and vehicle are calculated by the Newmark Method. The time step, parameters of Newmark Method and the error for convergence are determined before the iteration. Set the initial values $\mathbf{Q_0}$ and $\mathbf{Z_0}$.

Step 5: Determine the initial vehicle position on the bridge deck.

Step 6: Calculate the excitation force on vehicle, $\mathbf{F}_v^{int}$, from equation (11) and Appendix A, and solve for the motion of the vehicle, $\mathbf{Z}$, at time t from equation (10).

Step 7: Calculate the excitation force on the bridge, $\mathbf{F}_b^{int}$, from Appendix A, and solve for the motion of the bridge, $\mathbf{Q}$, at time t from equation (5).

Step 8: Solve for the displacement of the bridge $w(x, t)$ from equation (4).

Step 9: Repeat Steps 6–8 using the calculated $\mathbf{Q}$ and $\mathbf{Z}$. Check the convergence of the difference between the two successively calculated $w(x, t)_i$ and $w(x, t)_{i+1}$,

$$\|w(x, t)_{i+1} - w(x, t)_i\| \leqslant \textit{tolerance error}.$$

Step 10: If convergence is not achieved, repeat Steps 6–9. If convergence is achieved, repeat Steps 5–10 for the next time step.

3. NUMERICAL SIMULATIONS

3.1. VERIFICATION OF THE PROPOSED METHOD

The bridge–vehicle system in Maechesiello *et al.* [8] is used to verify the theory and the algorithm developed in the paper. No published results on an orthotropic plate can be found for comparison, and this isotropic plate [8] is used instead. The bridge is simplified into a continuous three-span isotropic plate with line intermediate rigid supports. The vehicle body is rigid and subject to bounce, pitch and roll motions. The parameters of the vehicle–bridge system are listed as follows:

$l_1 = l_2 = l_3 = 26{\cdot}4\,\text{m}$, $b = 10{\cdot}7\,\text{m}$, $h = 0{\cdot}95\,\text{m}$, $E = 14{\cdot}54 \times 10^{10}\,\text{N/m}^2$, $v = 0{\cdot}3$,

$\rho = 2375\,\text{kg/m}^2$, $S_x = 4{\cdot}73\,\text{m}$, $a_1 = 0{\cdot}67$, $a_2 = 0{\cdot}33$, $S_{d1} = S_{d2} = 2{\cdot}05\,\text{m}$, $S_{y1} = S_{y2} = 1{\cdot}41\,\text{m}$,

$m_c = 17\,000\,\text{kg}$, $m_{a1} = 600\,\text{kg}$, $m_{a2} = 1000\,\text{kg}$, $I_c = 9 \times 10^4\,\text{kg m}^2$, $I_t = 1{\cdot}3 \times 10^4\,\text{kg m}^2$,

$I_{a1} = 550\,\text{kg m}^2$, $I_{a2} = 600\,\text{kg m}^2$,

$K_{sy1} = K_{sy2} = 1{\cdot}16 \times 10^5\,\text{N/m}$, $\quad K_{sy3} = K_{sy4} = 3{\cdot}73 \times 10^5\,\text{N/m}$,

$K_{ty1} = K_{ty2} = 7{\cdot}85 \times 10^5\,\text{N/m}$, $\quad K_{ty3} = K_{ty4} = 1{\cdot}57 \times 10^6\,\text{N/m}$,

$C_{sy1} = C_{sy2} = 2{\cdot}5 \times 10^4\,\text{N s/m}$, $\quad C_{sy3} = C_{sy4} = 3{\cdot}5 \times 10^4\,\text{N s/m}$,

$C_{ty1} = C_{ty2} = 100\,\text{N s/m}$, $\quad C_{ty3} = C_{ty4} = 200\,\text{N s/m}$.

I_{a1} and I_{a2} are the torsional moments of inertia of the two axles, respectively; S_{y1} and S_{y2} are the spacing of the suspensions of the front and rear axle, respectively; the subscript *syi* refers to the *i*th suspension of the vehicle.

The natural frequencies of the continuous three-span isotropic plate are shown in Table 1. The results obtained by the proposed method are very close to that obtained using Zhou's method [17], and are approximately equal to the results in Marchesiello *et al.* [8].

TABLE 1

Natural frequencies for the three-span continuous bridge (Hz)

		Marchesiello *et al.* [8]		Zhou's method [17]		Proposed method	
Mode	Beam model	9 × 5*	17 × 9*	9 × 5*	17 × 9*	9 × 5*	17 × 9*
1	4·71	4·79	4·77	4·90	4·88	4·90	4·88
2	6·04	6·19	6·17	6·30	6·28	6·29	6·27
3	8·82	9·11	9·09	9·26	9·20	9·21	9·18
4	—	16·65	16·65	15·05	15·04	15·04	15·03
5	—	17·55	17·53	16·00	15·95	15·95	15·92
6	18·85	19·37	19·31	18·21	17·97	17·98	17·91
7	—	19·57	19·51	19·68	19·61	19·67	19·60
8	21·49	22·16	22·10	22·59	22·40	22·44	22·37

Note: 9 × 5* denotes 9 number of eigenfunctions in $\varphi_m(x)$ and 5 number of eigenfunctions in $\psi_n(y)$, and so on.

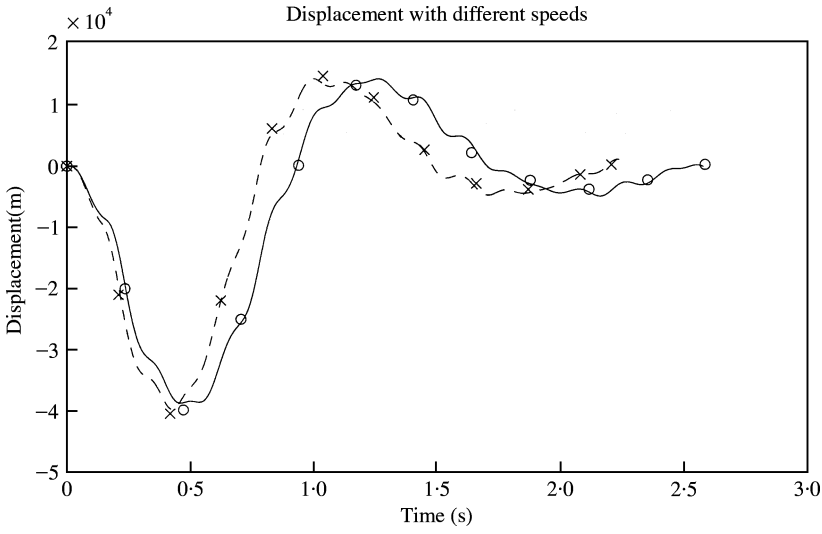

Figure 3. Displacements at different vehicle speed: ——, 32·5 m/s proposed; ○, Marchesiello *et al.*; – –, 37·5 m/s proposed; ×, Marchesielo *et al.*

This shows that the proposed method and algorithm to obtain the natural frequencies of the continuous plate are correct.

Another check is made on the accuracy of the computed response time histories. The vehicle moves along the edge with its right tyres at a distance 1·0 m from the right edge of the bridge. The displacements at the middle of the first span when the vehicle is moving at speeds of 32·5 and 37·5 m/s are shown in Figure 3. The first 13 modes are used in the calculation with a time step of 0·001 s. Comparison between the results obtained by the proposed method and those in Marchesiello *et al.* [8] show that the method and algorithm proposed in the paper are accurate to analyze the dynamic responses of a continuous multi-lane bridge deck under a moving vehicle.

3.2. MULTIPLE VEHICLES ON MULTI-LANE CONTINUOUS BRIDGE DECK

Not many studies have been done with multiple vehicles on top of a multi-lane bridge deck. Humar and Kashif [19] simplified a slab-type bridge as a single span orthotropic plate, and the effects of off-center vehicle and two vehicles on the bridge are discussed with a one-quarter vehicle model. Effects of having multiple vehicles on a single span bridge deck with two lanes have been presented by Yener and Chompooming [20]. Mabsout *et al.* [21] have also studied the effect of multi-lanes on the wheel distribution in a steel girder bridge.

A continuous three span multi-girder bridge as shown in Figure 4 is used for this study. There are four equal lanes over the total width of the bridge deck. The parameters of the bridge deck are listed as follows:

Span lengths are 24, 30, 24 m for the first, second and third spans, respectively; distance between two adjacent main girders is 2·743 m; distance between two adjacent diaphragms is 6 m; deck slab thickness is 0·2 m, $b = 13{\cdot}715$ m, $\rho = 3000\,\mathrm{kg/m^3}$, $E_x = 4{\cdot}1682 \times 10^{10}\,\mathrm{N/m^2}$ $E_y = 2{\cdot}9733 \times 10^{10}\,\mathrm{N/m^2}$, $v_{xy} = 0{\cdot}3$. For the steel I-beam: web thickness = 0·01111 m, web height = 1·490 m, flange width = 0·405 m, flange thickness = 0·018 m. For the diaphragms: cross-sectional area $= 0{\cdot}001548\,\mathrm{m^2}$, $I_y = 0{\cdot}707 \times 10^{-6}\,\mathrm{m^4}$, $I_z = 2 \times 10^{-6}\,\mathrm{m^4}$, $J = 1{\cdot}2 \times 10^{-7}\,\mathrm{m^4}$.

The rigidities of the equivalent orthotropic plate can be calculated according to Bakht and Jaeger [16] with $D_x = 2{\cdot}415 \times 10^9\,\mathrm{N\,m}$, $D_y = 2{\cdot}1807 \times 10^7\,\mathrm{N\,m}$, $D_{xy} = 1{\cdot}1424 \times 10^8\,\mathrm{N\,m}$. The first 13 natural frequencies of the continuous bridge are 4·13, 4·70, 6·31, 6·86, 7·76, 8·20,

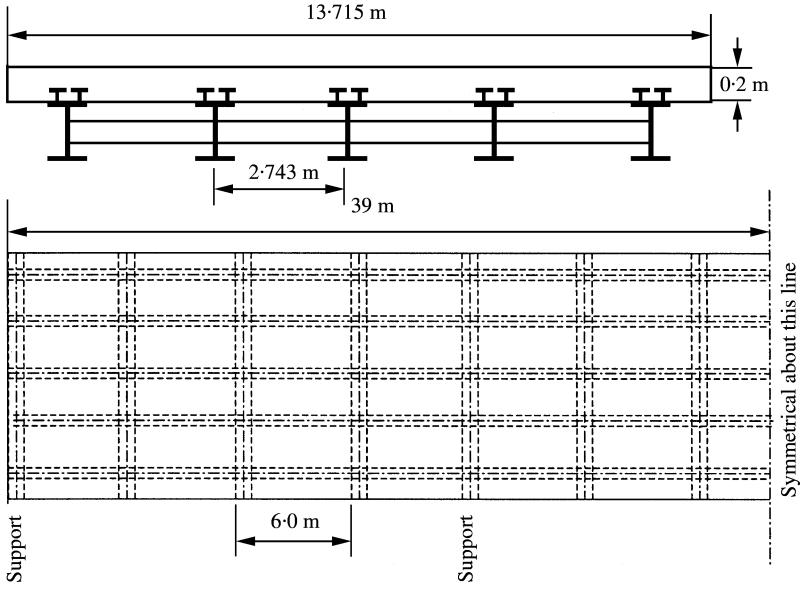

Figure 4. Diagram of the bridge.

15·81, 16·39, 20·84, 22·29, 22·90, 24·31 and 24·86 Hz. The damping coefficients of the bridge are taken as 0·02 for all the vibration modes. Road Classes A–D according to ISO-8608 [18] and the case without roughness are used in the simulations. The parameters of the vehicle are the same as those in section 3.1.

3.2.1. *Dynamic loading from a single vehicle*

The bending moment and shear force in the plate are calculated as

$$M_x = -\left(D_x \frac{\partial^2 w}{\partial x^2} + v_{xy} D_y \frac{\partial^2 w}{\partial y^2}\right),$$
$$V_x = -\left[D_x \frac{\partial^3 w}{\partial x^3} + (v_{xy} D_y + 4D_{xy}) \frac{\partial^3 w}{\partial x \partial y^2}\right]. \tag{15}$$

The impact factor and wheel-load distribution factor are defined after Huang *et al.* [2] as follows:

$$I_p = \left(\frac{R_d}{R_S} - 1\right) \times 100\%, \qquad \eta = \frac{M_i}{M_t}, \tag{16}$$

where R_d and R_S are the absolute maximum response from the dynamic and static studies respectively. Here R_S is obtained with the vehicle moving at a very low speed of 0·1 m/s with 0·1 s for the time step in the calculation and no road surface roughness is included. M_i is the maximum bending moment of one beam at the section; $M_t = M/n$; where M is the sum of the bending moment of all beams at one section; n is the number of wheel loads in the transverse direction.

Table 2 shows the static wheel load distribution, dynamic wheel load distribution and the impact factor from bending moment, displacement and strain under different loading cases.

TABLE 2

Load distribution factor(LDF) and impact factor(IMP) (for one vehicle load)

	Span	Load case	Beam-1	Beam-2	Beam-3	Beam-4	Beam-5
Static LDF	First	1	0·863	0·575	0·320	0·078	0·165
		2	0·586	0·486	0·395	0·309	0·224
		3	0·384	0·393	0·400	0·408	0·415
	Second	1	0·874	0·567	0·319	0·087	0·153
		2	0·564	0·509	0·405	0·305	0·217
		3	0·375	0·407	0·405	0·404	0·409
	Third	1	0·863	0·576	0·319	0·078	0·164
		2	0·587	0·487	0·394	0·309	0·224
		3	0·384	0·393	0·400	0·408	0·415
Dynamic LDF	First	1	0·850	0·568	0·319	0·091	0·172
		2	0·583	0·484	0·395	0·311	0·227
		3	0·384	0·393	0·400	0·408	0·415
	Second	1	0·864	0·561	0·320	0·098	0·157
		2	0·557	0·505	0·405	0·309	0·225
		3	0·376	0·407	0·405	0·404	0·409
	Third	1	0·856	0·572	0·317	0·085	0·170
		2	0·586	0·486	0·394	0·309	0·224
		3	0·384	0·393	0·400	0·408	0·415
IMP (%) (bending moment)	First	1	2·54	2·87	3·76	21·90	8·73
		2	2·90	3·16	3·54	4·11	5·15
		3	3·59	3·52	3·50	3·45	3·41
	Second	1	2·91	3·13	4·47	16·60	6·61
		2	2·48	2·92	3·75	5·14	7·51
		3	4·00	3·70	3·66	3·63	3·56
	Third	1	5·07	5·13	5·33	15·87	9·63
		2	5·25	5·25	5·27	5·32	5·40
		3	5·29	5·29	5·25	5·27	5·27
IMP (%) (displace-ment)	First	1	2·53	2·81	3·59	21·48	7·26
		2	2·81	3·03	3·36	3·89	4·85
		3	3·42	3·36	3·32	3·29	3·26
	Second	1	3·56	4·04	4·83	14·41	6·41
		2	3·45	3·34	3·97	5·11	7·12
		3	4·19	3·90	3·89	3·90	3·86
	Third	1	4·50	4·51	4·55	17·21	10·89
		2	4·56	4·53	4·50	4·47	5·53
		3	4·49	4·48	4·49	4·49	4·50
IMP (%) (strain)	First	1	2·54	2·87	3·76	21·85	8·74
		2	2·90	3·16	3·53	4·11	5·15
		3	3·59	3·53	3·49	3·45	3·42
	Second	1	2·91	3·13	4·46	16·61	6·58
		2	2·48	2·92	3·75	5·14	7·52
		3	4·00	3·71	3·66	3·63	3·56
	Third	1	5·08	5·15	5·30	15·98	9·68
		2	5·25	5·25	5·27	5·30	5·40
		3	5·27	5·26	5·26	5·27	5·26

The Loading Cases from a single vehicle are shown in Figure 5(a). Figure 6 shows the time histories of the bending moments, strains, shear forces and displacements at middle of the second span of beam-1 from Load Cases 1–3. Figure 7 shows the bending moments at

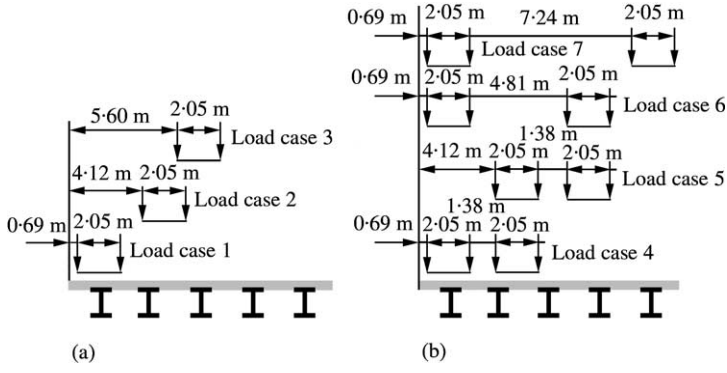

Figure 5. Vehicle loading: (a) one vehicle loading; (b) two vehicles loading.

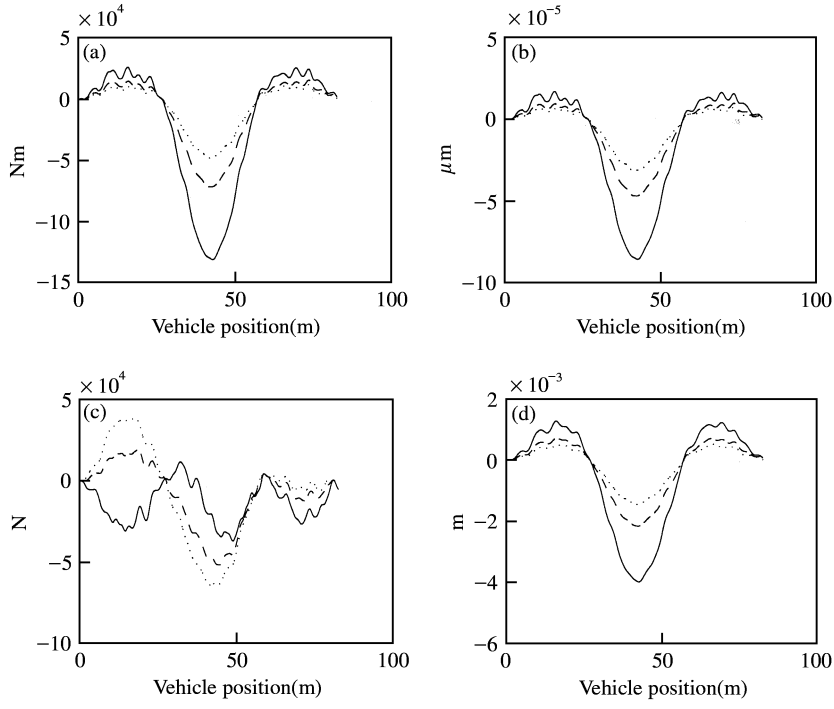

Figure 6. Responses at middle of Span 2 of Beam-1 under different loading: (a) Bending moment; (b) strain; (c) shear force; (d) displacement. ——, Load Case 1; – –, Load Case 2; …., Load Case 3.

middle of each span of each beam under Load Case 1. The speed of the vehicle is 30 m/s, and a time step of 0·001 s is used in the calculation. The road surface roughness is of Class B. Figures 8 and 9 show the effects of moving speed and the road surface roughness on the impact factors calculated at different points of the bridge deck under different loading cases. The legends 1–3, 4–5, 6–9, 10–12 and 13–15 define the midpoints of the first, second and third spans on beams 1–5 respectively. The following observations are obtained from these figures and Table 2.

(1) The dynamic impact factor calculated at different locations on the bridge deck varies in an opposite manner to that for the wheel load distribution factor. The former has

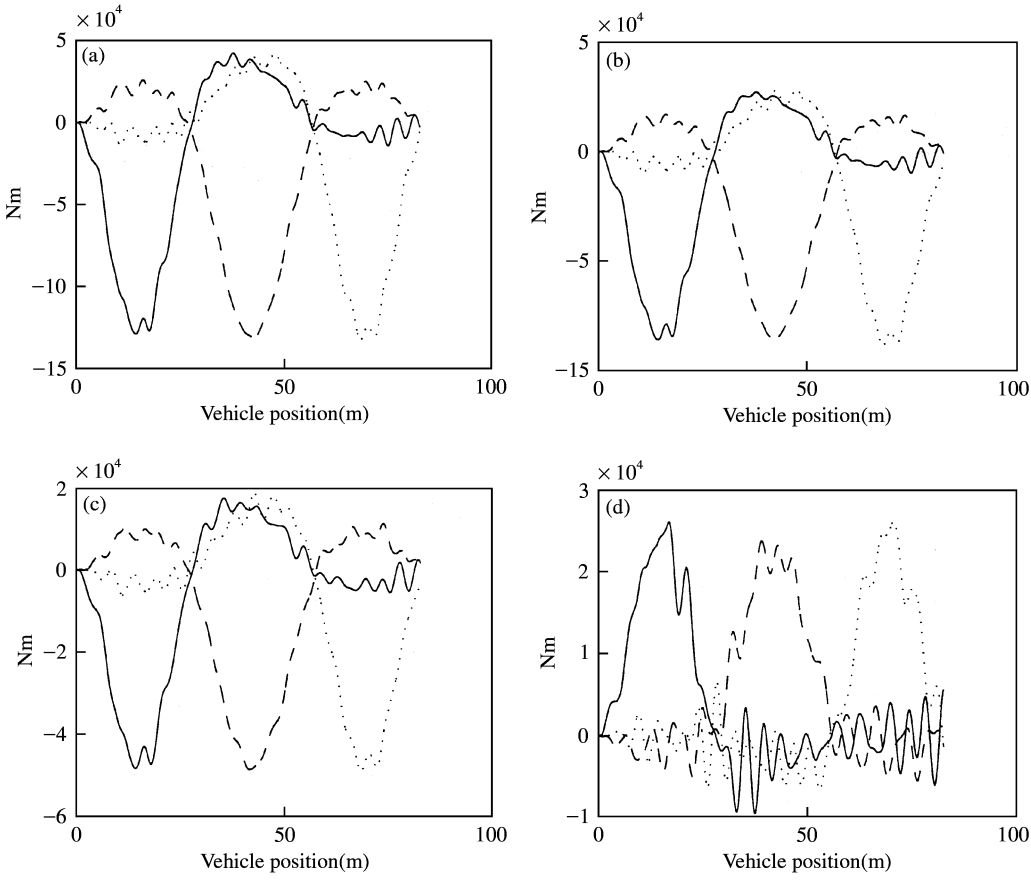

Figure 7. Bending moment at middle of each beam under Load Case 1: (a) Beam-1; (b) beam-2; (c) beam-3; (d) beam-5. ——, First span; – – –, second span; ....., third span.

a large value whereas the latter has a small value at the same point, and *vice versa*.

(2) The impact factors obtained from different measurable variables, such as bending moment, strain and displacement, are similar, and hence strains can be used in further studies as they can be easily measured.

(3) The bending moments in beams 1 and 2 are larger when the vehicle is close to them while those in beams 4 and 5 are smaller. This is because the motion of the vehicle in the outer lane excites the torsional modes which are significant to the responses.

(4) The impact factors on the beams near to the path of the moving vehicle are smaller than those in the beams further away. But the dynamic responses behave oppositely as seen in Figure 6.

(5) The impact factor is insensitive to the moving speed of the vehicle.

(6) In Load Case 1, the impact factors on beams 4 and 5 are larger than those in the other beams. The impact factors on beam 4 are largest in all the cases studied. This may be due to the torsional mode excited in Load Case 1.

(7) When the road surface roughness is increasing, the impact factors also increase especially for the case under eccentric Load Case 1. The maximum impact factor is 225% as seen in Figure 9.

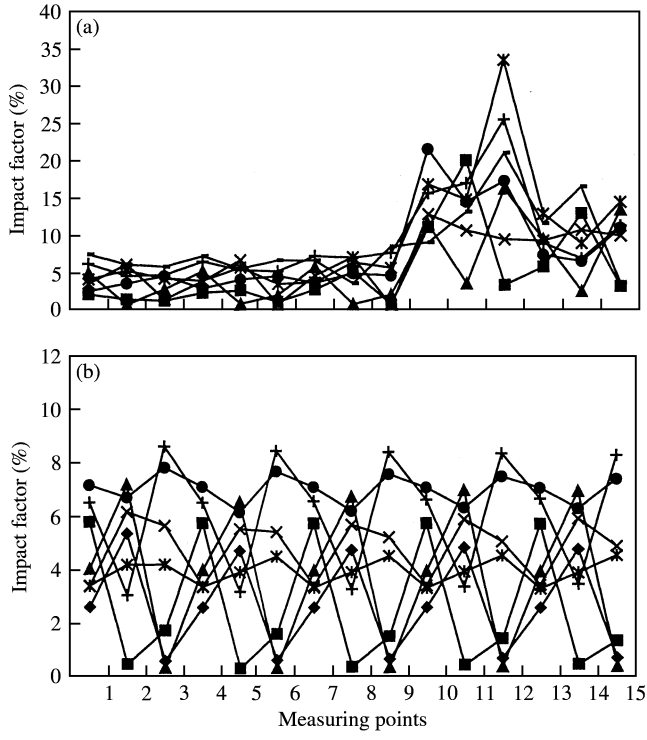

Figure 8. Effects of moving speed on impact factor: (a) effects under Load Case 1: —■—, 10 m/s; —▲—, 15 m/s; —×—, 20 m/s; —✳—, 25 m/s; —●—, 30 m/s; —+—, 35 m/s; ———, 40 m/s. (b) effects under Load Case 3: —◆—, 10 m/s; —■—, 15 m/s; —▲—, 20 m/s; —×—, 25 m/s; —✳—, 30 m/s; —●—, 35 m/s; —+—, 40 m/s.

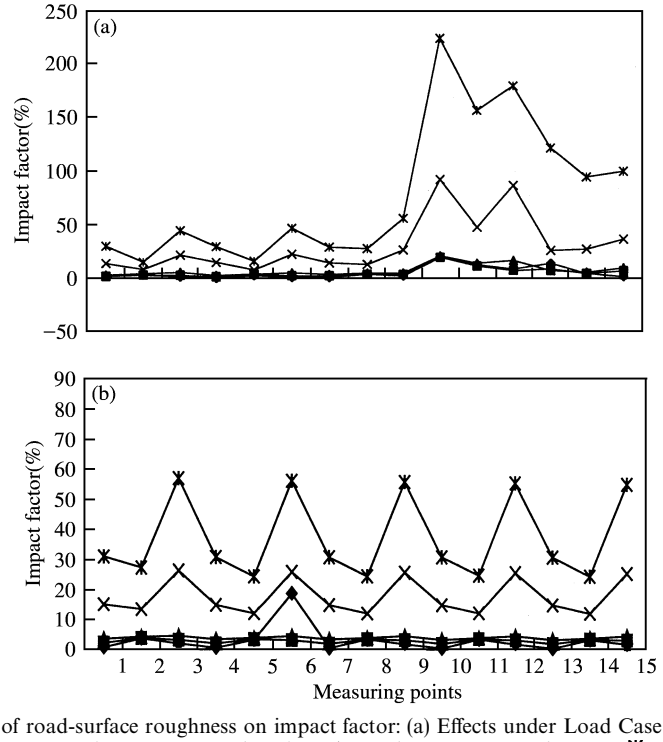

Figure 9. Effects of road-surface roughness on impact factor: (a) Effects under Load Case 1; (b) Effects under Load Case 3: —◆—, no roughness; —■—, Class A; —▲—, Class B; —×—, Class C; —✳—, Class D.

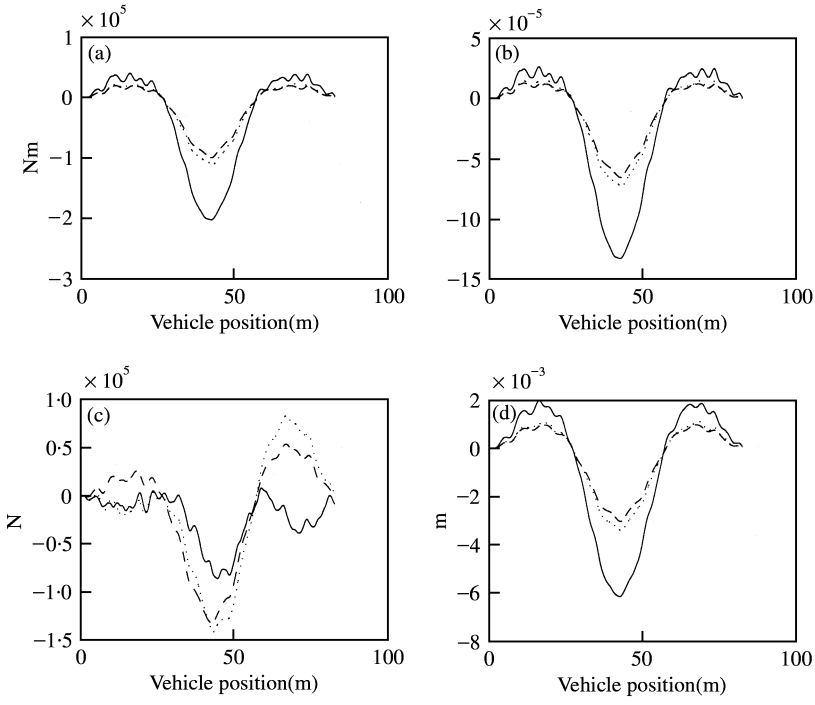

Figure 10. Responses at mid-point of Span 2 of Beam-1 under different loading. (a) Bending moment; (b) Strain; (c) shear force; (d) displacement. ——, Load Case 4; – – –, Load Case 5; · · · · ·, Load Case 7.

3.2.2. *Dynamic loading from multiple vehicles*

Two vehicles moving in different lanes are studied in the simulations. The loading cases are shown in Figure 5(b). Load Case 4 consists of two vehicles moving in the same direction. Load Cases 5–7 consist of two vehicles moving in opposite directions. Figure 10 shows the bending moments, strains, shear forces and displacements at midspan of span 2 of beam-1 under different loading cases. The speed of moving vehicles is 30 m/s, and the two vehicles enter the bridge at the same time. The road surface roughness is of Class *B*. Time step in the computation is 0·001 s. Figure 11 show the bending moments at middle of span 2 of beams 2, 3, 4 and 5 under the four loading cases. Table 3 shows the computed static and dynamic load distribution factor and impact factor. The following observations are made from these figures and Table 3.

(1) Tables 2 and 3 show that the impact factor generated from two vehicles is smaller than that from a single vehicle.
(2) The impact factor also behaves oppositely when compared with the wheel load distribution factor.
(3) The magnitude of bending moments in each beam is closely related to the transverse location of the resultant of the vehicular loads on the bridge deck. It is large when the resultant is close to the beam, and small when the force is further away from the beam.
(4) Loading No. 4 gives the largest impact factors in beam-5 which are 125·19, 120·82 and 92·60% at the middle of spans 1, 2 and 3 respectively. But the corresponding load distribution factor and the responses in Figure 11 are small. This is similar to the observation in point (6) made for a single vehicle in section 3.2.1 where the contribution of torsional modes of the bridge deck is suspected. This indicates a point

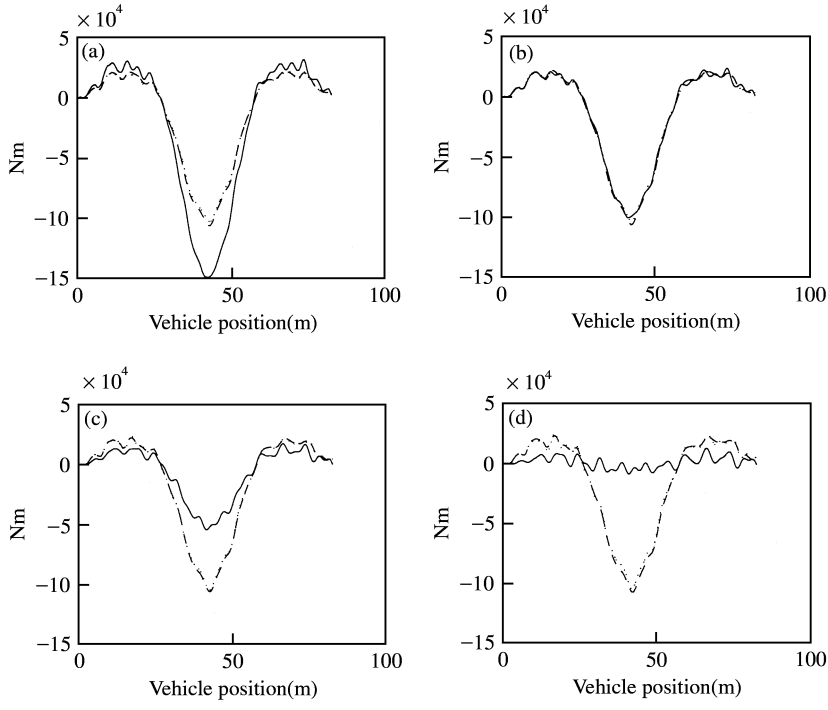

Figure 11. Bending moment at Beams 2 to 5 under different loading. (a) Beam-2; (b) beam-3; (c) beam-4; (d) beam-5. ——, Load Case 4; – – –, Load Case 5; ·····, Load Case 7.

that is often mixed up in design. The magnitude of the dynamic impact factor is of no significance if it is not related to the magnitude of stress or member capacity. A high impact factor, in general, corresponds to very low stress level. And only impact factors that relate to design situation are of importance.

(5) The impact factors differ significantly in the three spans under different loading. This would indicate a need to have different impact factors for the three spans in the design unless a conservative design is desired.

4. CONCLUSIONS

The design loading from vehicles moving on top of a three-dimensional continuous bridge deck has been investigated. The proposed method for analyzing the problem is based on a Lagrangian formulation of the vehicle–bridge system which is solved with the orthotropic plate theory and modal superposition technique. Numerical simulations have been performed to study the variation of dynamic impact factor and wheel load distribution factor on the bridge deck, and the following conclusions are obtained.

(1) The transverse vehicle position has an important effect on the impact factor. The impact factors in the beam that is far away from the path of the moving vehicle are larger than those that are near. But it is the opposite with the responses and wheel load distribution factor which are larger at points close to the moving vehicle.

(2) The high dynamic impact factors reported in this study correspond to low response level in the bridge deck and hence low stress level. Therefore, these impact factors

TABLE 3

Load distribution factor(LDF) and impact factor(IMP) (for two vehicle loads)

	Span	Load case	Beam-1	Beam-2	Beam-3	Beam-4	Beam-5
Static LDF	First	4	1·604	1·163	0·771	0·399	0·062
		5	0·896	0·756	0·644	0·783	0·921
		6	1·267	0·858	0·523	0·625	0·726
		7	1·072	0·730	0·460	0·734	1·005
	Second	4	1·593	1·176	0·781	0·407	0·043
		5	0·757	0·815	0·809	0·806	0·814
		6	1·222	0·973	0·781	0·604	0·420
		7	0·852	0·790	0·785	0·791	0·782
	Third	4	1·607	1·167	0·769	0·399	0·059
		5	0·895	0·751	0·648	0·784	0·922
		6	1·268	0·857	0·522	0·626	0·727
		7	1·072	0·725	0·462	0·735	1·007
Dynamic LDF	First	4	1·565	1·138	0·760	0·400	0·138
		5	0·900	0·765	0·642	0·778	0·916
		6	1·275	0·868	0·519	0·618	0·720
		7	1·071	0·737	0·460	0·731	1·001
	Second	4	1·558	1·152	0·775	0·420	0·095
		5	0·754	0·810	0·808	0·808	0·820
		6	1·201	0·964	0·780	0·614	0·441
		7	0·838	0·783	0·784	0·797	0·798
	Third	4	1·584	1·151	0·760	0·395	0·110
		5	0·915	0·772	0·658	0·761	0·894
		6	1·296	0·881	0·522	0·604	0·697
		7	1·094	0·747	0·456	0·719	0·985
IMP (%) (displacement)	First	4	2·66	2·93	3·50	5·27	125·19
		5	0·78	1·26	0·29	0·21	0·16
		6	1·42	1·61	0·31	− 0·09	− 0·30
		7	0·33	0·91	0·25	− 0·12	− 0·30
	Second	4	3·02	3·17	4·00	7·17	120·82
		5	6·48	5·99	6·42	6·90	7·20
		6	4·94	5·93	6·88	8·39	11·60
		7	5·14	6·27	6·84	7·55	8·61
	Third	4	4·67	4·68	4·70	5·91	92·60
		5	6·22	6·93	5·34	0·88	0·61
		6	5·64	6·39	2·99	− 0·73	0·34
		7	4·81	5·86	1·14	0·12	− 0·15

should be taken with care as only when they are related to the design situation that they would be of importance.

(3) The impact factors associated with multiple vehicles are smaller than those for single vehicle.

(4) The road surface roughness is more important to the impact factors than the moving speed of the vehicle.

ACKNOWLEDGMENT

The work described in this paper was supported by a grant from the Hong Kong Polytechnic University Research Funding Project No. V653.

REFERENCES

1. *AASHTO LRFD Bridge Design Specifications* 1998 American Association of State Highway and Transportation Officials.
2. D. Z. Huang, T. L. Wang and M. Shahawy 1992 *Journal of Structural Engineering American Society of Civil Engineers* **118**, 3427–3443. Impact analysis of continuous multigirder bridges due to moving vehicles.
3. T. L. Wang, D. Z. Huang and M. Shahawy 1992 *Journal of Structural Engineering American Society of Civil Engineers* **118**, 2222–2238. Dynamic response of multi-girder bridges.
4. M. F. Green and D. Cebon 1994 *Journal of Sound and Vibration* **170**, 51–78. Dynamic response of highway bridges to heavy vehicle loads: theory and experimental validation.
5. P. K. Chatterjee, T. K. Datta and C. S. Surana 1994 *Journal of Sound and Vibration* **169**, 619–632. Vibration of continuous bridges under moving vehicles.
6. K. Chompooming and M. Yener 1995 *Journal of Sound and Vibration* **183**, 567–589. The influence of roadway surface irregularities and vehicle deceleration on bridge dynamics using the method of lines.
7. F. H. Yang and G. A. Fonder 1996 *Earthquake Engineering and Structural Dynamics* **25**, 195–215. An iterative solution method for dynamic response of bridge-vehicles systems.
8. S. Marchesiello, A. Fasana, L. Garibaldi and B. A. D. Piombo 1999 *Journal of Sound and Vibration* **224**, 541–561. Dynamics of multi-span continuous straight bridges subject to multi-degrees of freedom moving vehicle excitation.
9. S. S. Law and X. Q. Zhu 2000 *Journal of Bridge Engineering American Society of Civil Engineers* (submitted). Effects of vehicle braking with road roughness on bridge deck.
10. K. Henchi, M. Fafard, M. Talbot and G. Dhatt 1998 *Journal of Sound and Vibration* **212**, 663–683. An efficient algorithm for dynamic analysis of bridges under moving vehicles using a coupled modal and physical component approach.
11. Y.-B. Yang, C.-H. Chang and J.-D. Yau 1999 *International Journal for Numerical Methods in Engineering* **46**, 1031–1047. An element for analyzing vehicle-bridge systems considering vehicle's pitching effect.
12. R. Cantieni 1993 *Structural Dynamics—EURODYN*'93, 961–968. Vehicle/bridge dynamic interaction for highway bridges.
13. E.-S. Hwang and A. S. Nowak 1991 *Journal of Structural Engineering American Society of Civil Engineers* **117**, 1413–1434. Simulation of dynamic load for bridges.
14. Y.-B. Yang, S.-S. Liao and B.-H. Lin 1995 *Journal of Structural Engineering American Society of Civil Engineers* **121**, 1644–1650. Impact formulas for vehicles moving over simple and continuous beams.
15. J.-W. Kou and J. T. Dewolf 1997 *Journal of Structural Engineering American Society of Civil Engineers* **123**, 333–344. Vibrational behavior of continuous span highway bridge—influence variables.
16. B. Bakht and L. G. Jaeger 1985 *Bridge Analysis Simplified*. New York: McGraw-Hill.
17. D. Zhou 1994 *International Journal of Solids and Structures* **31**, 347–358. Eigenfrequencies of line supported rectangular plates.
18. *ISO* 8608:1995(E). Mechanical vibration—road surface profiles—reporting of measured data.
19. J. L. Humar and A. H. Kashif 1995 *Journal of Structural Engineering American Society of Civil Engineers* **121**, 48–62. Dynamic response analysis of slab-type bridges.
20. M. Yener and K. Chompooming 1994 *Computers and Structures* **53**, 709–726. Numerical method of lines for analysis of vehicle-bridge dynamic interaction.
21. M. E. Mabsout, K. M. Tarhini, G. R. Frederick and A. Kesserwan 1999 *Journal of Bridge Engineering American Society of Civil Engineers* **4**, 99–106. Effect of multi-lanes on wheel load distribution in steel girder bridges.

APPENDIX A: SYSTEM MATRICES

A.1. VEHICLE MODEL

$$\mathbf{Z} = \{y_c, \theta_p, \theta_r, y_{a1}, \theta_{a1}, y_{a2}, \theta_{a2}\}^{\mathrm{T}},$$

$$\mathbf{F}_v^{int} = \left\{0, 0, 0, -F_{t1} - F_{t2}, \frac{S_{d1}}{2}(F_{t1} - F_{t2}), -F_{t3} - F_{t4}, \frac{S_{d2}}{2}(F_{t3} - F_{t4})\right\}^{\mathrm{T}},$$

$\mathbf{M}_v = \text{diag}\{m_c, I_c, I_t, m_{a1}, I_{a1}, m_{a2}, I_{a2}\}$, $\mathbf{K}_v = \{K_{vij}, K_{vij} = K_{vji}, i = 1, 2, \ldots, 7;$

$j = 1, 2, \ldots, 7\}$,

$$K_{v11} = \sum_{i=1}^{4} K_{syi}, \qquad K_{v12} = (K_{sy1} + K_{sy2})a_1 S_x - (K_{sy3} + K_{sy4})a_2 S_x,$$

$$K_{v13} = \frac{S_{y1}}{2}(-K_{sy1} + K_{sy2}) + \frac{S_{y2}}{2}(-K_{sy3} + K_{sy4}), \qquad K_{v14} = -(K_{sy1} + K_{sy2}),$$

$$K_{v15} = \frac{S_{y1}}{2}(K_{sy1} - K_{sy2}), \qquad K_{v16} = -K_{sy3} - K_{sy4}, \qquad K_{v17} = \frac{S_{y2}}{2}(K_{sy3} - K_{sy4}),$$

$$K_{v22} = (K_{sy1} + K_{sy2})a_1^2 S_x^2 + (K_{sy3} + K_{sy4})a_2^2 S_x^2,$$

$$K_{v23} = \tfrac{1}{2}(-K_{sy1} + K_{sy2})a_1 S_x S_{y1} + \tfrac{1}{2}(K_{sy3} - K_{sy4})a_2 S_x S_{y2},$$

$$K_{v24} = -(K_{sy1} + K_{sy2})a_1 S_x, \quad K_{v25} = \tfrac{1}{2}(K_{sy1} - K_{sy2})a_1 S_x S_{y1},$$

$$K_{v26} = (K_{sy3} + K_{sy4})a_2 S_x, \quad K_{v27} = -\tfrac{1}{2}(K_{sy3} - K_{sy4})a_2 S_x S_{y2},$$

$$K_{v33} = \frac{S_{y1}^2}{4}(K_{sy1} + K_{sy2}) + \frac{S_{y2}^2}{4}(K_{sy3} + K_{sy4}),$$

$$K_{v34} = \frac{S_{y1}}{2}(K_{sy1} - K_{sy2}), \quad K_{v35} = -\frac{S_{y1}^2}{4}(K_{sy1} + K_{sy2}), \quad K_{v36} = \frac{S_{y2}}{2}(K_{sy3} - K_{sy4}),$$

$$K_{v37} = -\frac{S_{y2}^2}{4}(K_{sy3} + K_{sy4}),$$

$$K_{v44} = (K_{sy1} + K_{sy2}), \quad K_{v45} = \frac{S_{y1}}{2}(-K_{sy1} + K_{sy2}), \quad K_{v46} = K_{v47} = 0,$$

$$K_{v55} = \frac{S_{y1}^2}{4}(K_{sy1} + K_{sy2}), \quad K_{v56} = K_{v57} = 0,$$

$$K_{v66} = K_{sy3} + K_{sy4}, \quad K_{v67} = -\frac{S_{y2}}{2}(K_{sy3} - K_{sy4}), \quad K_{v77} = \frac{S_{y2}^2}{4}(K_{sy3} + K_{sy4}),$$

where S_{y1}, S_{y2} are the spacing of suspensions in the front and rear axles, respectively; S_x, is the axle spacing.

A.2. BRIDGE MODEL

$$\mathbf{Q} = \{q_1(t), q_2(t), \ldots, q_{M_n}(t)\}^{\mathrm{T}}, \mathbf{W} = \{W_1(x, y), W_2(x, y), \ldots, W_{M_n}(x, y)\},$$

M_n is the number of mode shapes for the continuous orthotropic plate.

$$M_b = \iint_S \rho h W^{\mathrm{T}} W \, \mathrm{d}S, \quad C_b = \iint_S c_b W^{\mathrm{T}} W \, \mathrm{d}S,$$

$$\mathbf{W}_b = \begin{bmatrix} W_1(\hat{x}_1(t), \hat{y}_1(t)) & W_1(\hat{x}_2(t), \hat{y}_2(t)) & \cdots & W_1(\hat{x}_{N_p}(t), \hat{y}_{N_p}(t)) \\ W_2(\hat{x}_1(t), \hat{y}_1(t)) & W_2(\hat{x}_2(t), \hat{y}_2(t)) & \cdots & W_2(\hat{x}_{N_p}(t), \hat{y}_{N_p}(t)) \\ \vdots & \vdots & \cdots & \vdots \\ W_{M_n}(\hat{x}_1(t), \hat{y}_1(t)) & W_{M_n}(\hat{x}_2(t), \hat{y}_2(t)) & \cdots & W_{M_n}(\hat{x}_{N_p}(t), \hat{y}_{N_p}(t)) \end{bmatrix},$$

$$\mathbf{K}_b = \iint_S \Big[D_x \mathbf{W}_x''^{T} \mathbf{W}_x'' + \frac{1}{2}(D_x v_{yx} + D_y v_{xy})(\mathbf{W}_x''^{\mathrm{T}} \mathbf{W}_y'' + \mathbf{W}_y''^{\mathrm{T}} W_x'') + D_y \mathbf{W}_y''^{\mathrm{T}} \mathbf{W}_y'' + 4 D_k \mathbf{W}_{xy}''^{\mathrm{T}} \mathbf{W}_{xy}'' \Big] \mathrm{d}S,$$

$$W_{xi}'' = \sum_m \sum_n A_{mn} \varphi_m''(x) \psi_n(y), \quad W_{xyi}'' = \sum_m \sum_n A_{mn} \varphi_m'(x) \psi_n'(y),$$

$$W_{yi}'' = \sum_m \sum_n A_{mn} \varphi_m(x) \psi_n''(y) \quad (i = 1, 2, \ldots, M_n)$$

$$\mathbf{F}_b^{int} = \mathbf{F}_g + \mathbf{F}_b, \quad \mathbf{F}_b = \{F_{t1}, F_{t2}, F_{t3}, F_{t4}\}^{\mathrm{T}},$$

$$\mathbf{F}_g = \{(m_c a_1 + m_{a1})g/2, (m_c a_1 + m_{a1})g/2, (m_c a_2 + m_{a2})g/2, (m_c a_2 + m_{a2})g/2\}^{\mathrm{T}},$$

where $\mathbf{F}_g$ is the force vector caused by the effect of gravitation.